TEM characterization of MnO_2 cathode in an aqueous lithium secondary battery

Manickam Minakshi[1]*, David Mitchell[2], Pritam Singh[1] and Stephen Thurgate[3]

[1]Division of Science and Engineering, Murdoch University, Murdoch 6150, Western Australia.
[2]Materials and Engineering Science, ANSTO Materials, PMB 1, Menai, NSW 2234, Australia.
[3]Dean, Division of Information and Communication Sciences, Macquarie University, NSW 2109, Australia

Abstract
The discharge characteristics of manganese dioxide cathode in the presence of small amounts (1, 3 and 5 wt. %) of titanium disulphide (TiS_2) additive has been investigated in an alkaline cell using aqueous lithium hydroxide as the electrolyte. The incorporation of small amounts of TiS_2 additives into manganese dioxide (MnO_2) was found to improve the battery discharge capacity from 150 to 270 mAh/g. However, increasing the additive from 3 to 5 wt. % causes a decrease in the discharge capacity. Hence, the objective is to gain insight into the role of TiS_2 in MnO_2 and its mechanism. For this purpose, we have used transmission electron microscopy (TEM), electron energy loss spectroscopy (EELS) and secondary ion mass spectrometry (SIMS). The valence state determination and the depth profile analysis of the discharged MnO_2 were performed using EELS and SIMS techniques.
Keywords: MnO_2, lithium intercalation, aqueous, secondary battery, TiS_2 additive.

Introduction
Alkaline cells with manganese dioxide cathodes are eminently suitable for a wide range of applications. They are inexpensive, operate at ambient temperature, have a long shelf-life and are capable of high discharge rates. Presently, the alkaline MnO_2/Zn system using traditional potassium hydroxide (KOH) as electrolyte is limited to primary batteries. This is because the electrochemical insertion of protons into the host MnO_2 is irreversible [3].
As the lithium batteries are hazardous, interest is now increasing in the development of such alkaline MnO_2 into rechargeable batteries [4]. However, the limitations connected with the inherent reversible character of $Mn^{4+}/^{2+}$ redox processes have been removed by using lithium chloride (LiCl) or lithium hydroxide (LiOH) as the electrolyte of fully rechargeable manganese dioxide materials [5-6]. With this aqueous LiOH electrolyte, during the discharge process, the MnO_2 forms an intercalation compound of the formula Li_xMnO_2 and we refer to this battery as an "aqueous lithium secondary battery" [6].
In the present work, we have investigated this reaction by transmission electron microscopy (TEM) and electron energy loss spectroscopy (EELS) techniques. Furthermore, the influence of titanium disulphide (TiS_2) as an additive in small amounts to the MnO_2 cathode has been characterized, in order to provide the mechanistic information. SIMS, TEM and associated techniques are necessary to provide information critical to a good material design.

Experimental
The γ-MnO_2 battery grade material used in this work was purchased from the Sigma Aldrich. Titanium disulphide (TiS_2) was obtained from Alfa Aesar. For the electrochemical test, a pellet was prepared by mixing 70-75 wt % MnO_2 consisting of 0-5 wt % TiS_2 with 20 wt % acetylene black (A-99, Asbury, USA) and 5 wt % poly (vinylidene difluoride) (PVDF, Sigma Aldrich) binder in a mortar and pestle. An electrochemical cell was constructed with the disk-like pellet as the cathode, Zn metal as the anode and filter paper as the separator. The electrolyte was a saturated solution of lithium hydroxide (LiOH) containing 1 $mol.l^{-1}$ zinc sulphate ($ZnSO_4$). The cell design and its experimental details were similar to those reported earlier [6]. The cells were discharged/charged galvanostatically at 0.3 mA/cm^2 by using an EG&G Princeton Applied Research Potentiostat/Galvanostat model 273 A, operated by model 270 software (EG&G). The cut-off discharge and charge voltages were 1.0 and 1.9 V, respectively. All electrochemical measurements were carried out in air at 25°C. The morphology and interplanar spacings of the products formed before and after discharge were characterized by transmission electron microscopy (TEM), high-resolution TEM (HRTEM) and electron energy loss spectroscopy (EELS) using a JEOL 2010F TEM model operated at 200kV. TEM specimens were prepared by grinding a small fragment scraped from the pressed pellet under methanol and dispersing on a holey carbon support film. Specimens were examined at liquid nitrogen temperature in a cooling stage, to reduce beam damage and contamination effects. Secondary Ion Mass Spectrometry (SIMS) spectra were collected on a Cameca ims 5f instrument at the Australian Nuclear Science and Technology Organization (ANSTO), Lucas Heights, Sydney. An O_2^+ primary ion source (12.5 KV) was used to generate secondary ions. A primary beam of 50 nA rastered over an area of 250 x 250μm was used in all experiments. The SIMS positive ion signals corresponding to ^7Li was recorded.

Results and Discussion

Additions of Bi^{3+} additive to MnO_2 has been shown to produce a slight improvement in the battery behavior, and several other additives have been explored [7-8]. A potential candidate in this regard has been Ti^{4+} ion [9]. In this work, small amounts of TiS_2 (1, 3 and 5 wt.%) as additives have been ground together with MnO_2 and their electrochemical behavior investigated. Figure 1 compares the discharge performance of the MnO_2 containing small amounts of TiS_2. For the plain MnO_2 (without additive) the observed capacity is 150 mAh/g. With 1 wt. % additive, there was an increase in capacity value from 150 to 175 mAh/g. With 3 wt. % additive, electrode capacity increased dramatically to 270 mAh/g, whereas, for a cell with 5 wt. % additive, capacity decreased to 75 mAh/g. Although the shape of the discharge curve remains unchanged for the various additive loadings, the average voltage is significantly reduced for 5 wt. % material. Fig. 2 compares the cycling performance of the Zn-MnO_2 cells for first ten cycles in the presence of 0, 3 and 5 wt % additive. The available capacity is low and decreases quickly for the 5 wt % additive. The plain MnO_2 cell shows significantly improved capacity although this is still less than that of 3 wt % additive. The cell capacity is high for 3 wt % additive and decreased gradually for the first 5 cycles (from 260 to 192 mAh/g, reflecting a loss of 25 %) then stabilized with a further loss of only 13 % at the 10^{th} cycle. Although the plain MnO_2 shows improved capacity retention during cycling, its energy density is lower than that of 3 wt% additive.

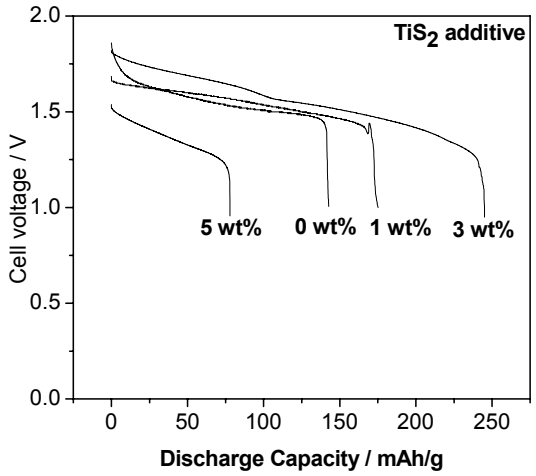

Fig. 1 Comparison of the first discharge profiles of MnO_2 in the presence of small amounts of TiS_2 additives (weight percent is indicated in the profiles).

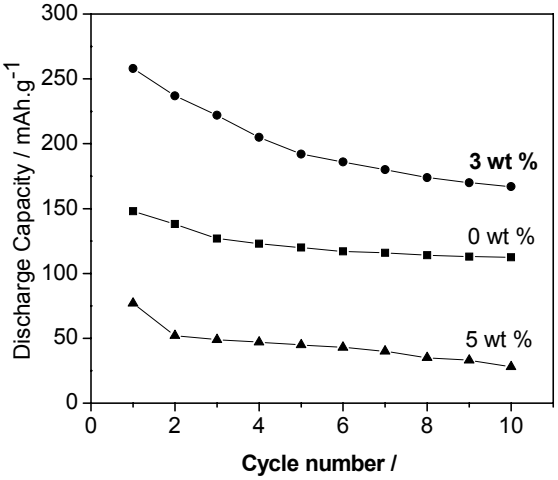

Fig. 2 Comparison of the discharge capacity versus cycle number for the Zn-MnO_2 cell in the presence of 0, 3 and 5 wt% additive

TEM examination of MnO_2 particles (Fig. 3) with small amounts of additives revealed that the size distribution of particles appeared finer in 1 wt. % compared with 3-5 wt. % albeit with the sampling issues associated with the TEM method. As expected TiS_2 particles are more apparent in the more highly loaded materials, this phase being conspicuous due to its plate-like morphology (Fig. 3).

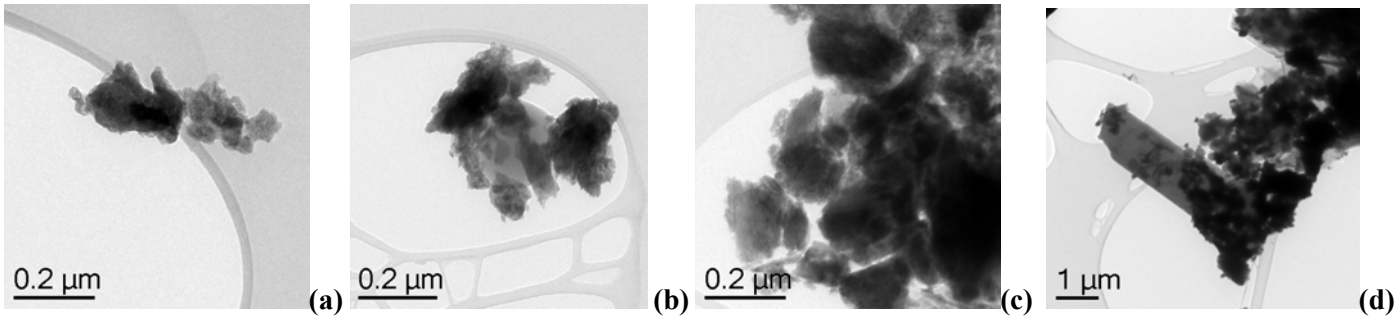

Fig. 3 TEM images showing particle morphology and size distribution of MnO_2 powder with TiS_2 additive (a) 1 (b) 3 (c) 5 and (d) enlarged image of 5 wt% (plate-like morphology).

EELS-Valence state determination

The EELS determination of valence state is possible due to the effect of the occupied electron orbital on the shape of the EELS peaks. In the case of Manganese, the Mn $L_{2,3}$ peak appears as a doublet. The relative intensities of these peaks vary as a function of valence state in the Mn oxides i.e. MnO, Mn_2O_3 and MnO_2. The parameter used to measure this ratio is called the branching ratio, defined as $I(L_3)/(I(L_2) + I(L_3))$ where L_2 and L_3 are the corresponding EELS lines [10]. The Mn L_3 edge occurs at 640eV and the L_2 edge at 651eV.

A typical EELS spectrum for the as-received MnO_2 is shown in Fig. 4. The mean branching ratio was found to be 0.678 ± 0.005, which agreed well with the previously determined value for a difference source of MnO_2 of 0.685 ± 0.01 [10]. Hence, the valence state of the MnO_2 starting material used in this work is + 4 as expected. The measured branching ratio/valence state of MnO_2 after discharge (lithium intercalated) was found to vary in a manner which reflected the discharge characteristics in Fig. 1. As can be seen in Fig. 5, the valence state of Mn decreased with TiS_2 loading up to a maximum at 3wt% TiS_2, and then increased at 5wt% TiS_2 loading. The discharged materials showed evidence for reduction, the extent of which depended on the amount of TiS_2 additive. The valance state of discharged MnO_2 with 3 wt. % TiS_2 additive was 3.1± 0.01 while that for the equivalent material with 5wt. % TiS_2 additive was 3.5± 0.01.

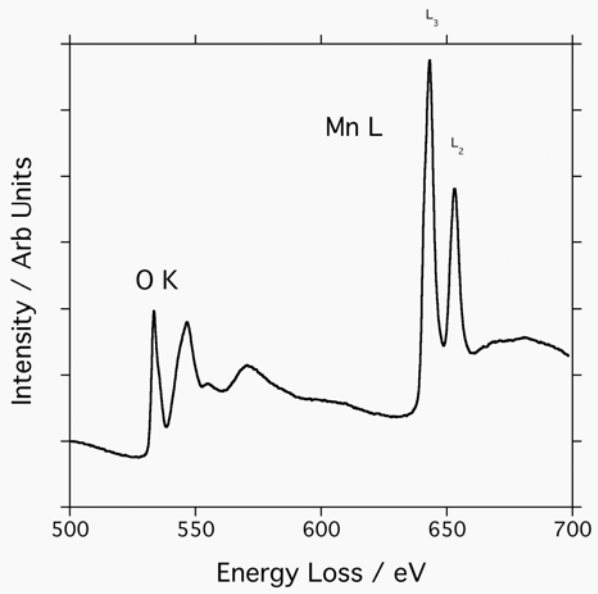

Fig. 4 EELS spectrum from MnO_2 as received. The O K edge is at 532eV and the Mn $L_{2,3}$ edge at 640eV.

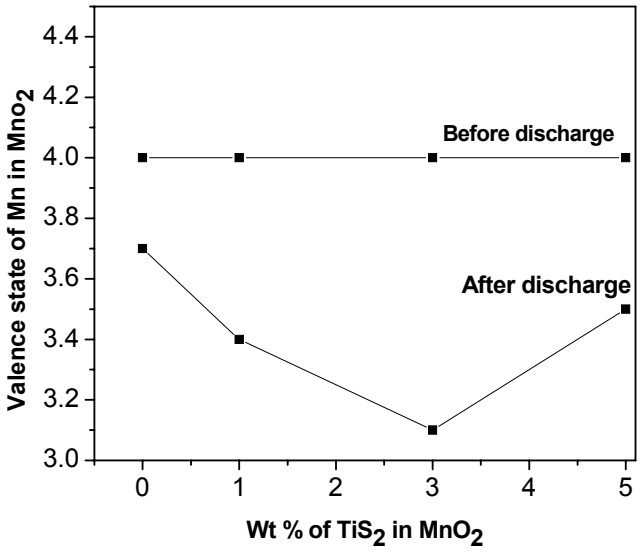

Fig. 5 Valence state of Mn in MnO_2 of before and after discharge for various wt. % of TiS_2 additives.

HRTEM images In order to understand the reduction mechanism HRTEM images of MnO_2 before and after discharge were obtained. The MnO_2 before discharge for 3 wt % showed very fine lattice fringes (Fig 6a) the largest of which were about 0.24 nm. Much larger lattice fringes were seen in the discharged form (Fig. 6b) with a mean spacing of about 0.45 nm. This indicates that the lattice is crystalline after discharge. While for 5 wt % discharged sample (Fig. 6c) fringes were far less intense and widespread.

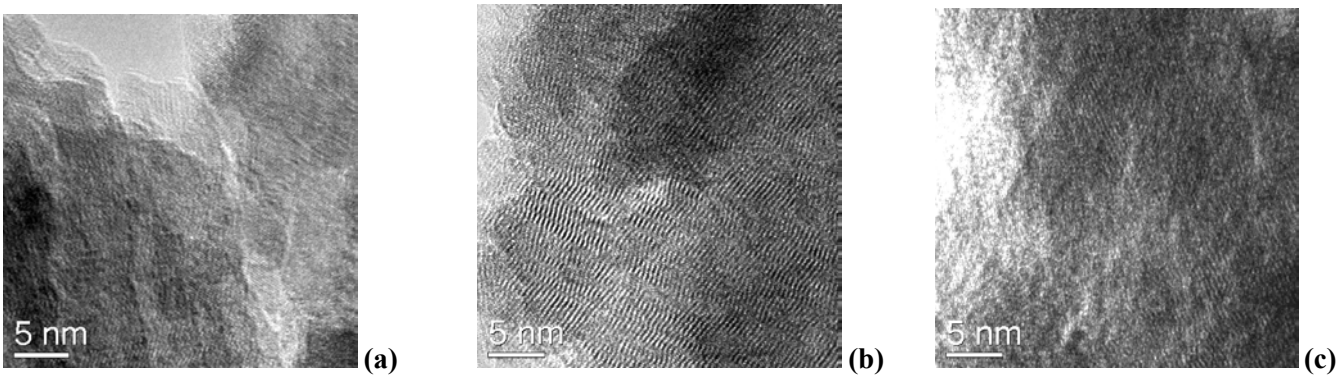

Fig. 6 HRTEM of MnO_2 cathode for 3 wt % (a) before, (b) after discharge and (c) 5 wt % after discharge.

The results of EELS and HRTEM images of MnO_2 with presence of additives are consistent with the electrochemical (discharge) behaviour as seen in Fig. 1 explaining that cell capacity increases with the threshold of 3 wt% then it decreases.

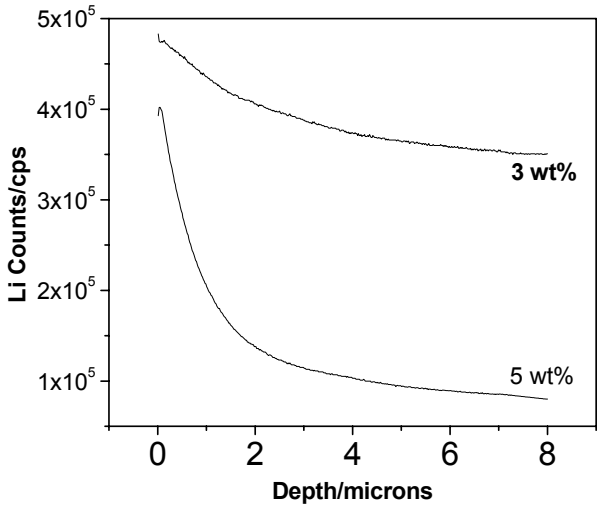

Fig. 7 SIMS depth profile analysis on the discharged MnO_2 cathode with 3 and 5 wt. % additives

To reveal the discharge mechanism in the 5 wt % additive, SIMS depth profile analysis were performed on the discharged cathode containing 5 wt % TiS_2 and compared with that of the 3 wt % additive. The SIMS analysis in Fig. 7 shows a dramatic decrease (approx. two orders of magnitude) of Li^+ ion count for 5 wt % additives. This confirms that the reduction of Mn occurs via Li intercalation, the extent being more marked for the 3 wt. % TiS_2 loading. TEM imaging of the 5 wt. % additive material showed a presence of a coating of nanoparticulate Mn oxyhydroxides, of about 50 nm diameter. This could inhibit the lithium intercalation (valence state 3.5± 0.01) and thereby explain the low discharge capacity of this material. Nano particulate material was not present in the 1 and 3 wt. % TiS_2 loaded material.

Conclusions

The zinc/manganese dioxide cell containing aqueous lithium hydroxide electrolyte undergoes a lithium intercalation into the host framework structure of the cathode material (MnO_2) during discharge and the process is reversible. Small amounts of TiS_2 additive into the MnO_2 cathode improve the discharge capacity. However, increasing the additive content above 3 wt % causes a decrease in the cell voltage and discharge capacity. The valence state determination using EELS and lattice imaging of TEM confirmed that reduction of Mn occurs as a result of Li intercalation. SIMS depth profile analysis supports the lithium intercalation mechanism.

Acknowledgements

Murdoch University is acknowledged for providing funding under Research Excellence Grant Scheme (REGS). The Australian Institute for Nuclear Science and Engineering is also acknowledged for providing grant to carry out some of the work at ANSTO laboratories, Lucas heights, New South Wales.

References

1. Y. F. Yao, U.S. Patent No. 4,520,005 (1985).
2. Y. F. Yao, N.K. Gupta and H.S. Wroblowa, J. Electro anal. Chem., 223 (1987) 107.
3. K. Kordesch, J. Gsellmann, M. peri, K. Tomantschger and R.Chemelli, Electrochim. Acta, 26 (1981) 1495.
4. Y. Hom, J. Takao, and H. Shomon, Electrochim. Acta, 30 (1985) 1121.
5. R.L. Deutscher, T.M. Florence and R. Woods, J. Power Sources, 55 (1995) 41.
6. Manickam Minakshi, Pritam Singh, Touma B. Issa, Stephen Thurgate and Roland DeMarco, J. Power Sources, 130 (2004) 285.
7. S.W. Donne, G.A. Lawrence and D.A.J. Swinkels, J. Electrochem. Soc., 144, 2954 (1997).
8. H. S. Wroblowa and N. Gupta, J. Electroanal. Chem., 238, 93 (1987).
9. V. K. Nartey, L. Binder and A. Huber, J. Power Sources 87, 205 (2000).
10. T. Riedl, T. Gemming and K. Wetzig, Ultramicroscopy, 106 (2006) 284-291.